Proc. Natl. Acad. Sci. USA
Vol. 93, pp. 21–26, January 1996

Review

Protein–protein interactions in the rigor actomyosin complex

Ronald A. Milligan

Department of Cell Biology, The Scripps Research Institute, 10666 North Torrey Pines Road, La Jolla, CA 92037

ABSTRACT **Since it has not been possible to crystallize the actomyosin complex, the x-ray structures of the individual proteins together with data obtained by fiber diffraction and electron microscopy have been used to build detailed models of filamentous actin (f-actin) and the actomyosin rigor complex. In the f-actin model, a single monomer uses 10 surface loops and two α-helices to make sometimes complicated interactions with its four neighbors. In the myosin molecule, both the essential and regulatory light chains show considerable structural homology to calmodulin. General principles are evident in their mode of attachment to the target α-helix of the myosin heavy chain. The essential light chain also makes contacts with other parts of the heavy chain and with the regulatory light chain. The actomyosin rigor interface is extensive, involving interaction of a single myosin head with regions on two adjacent actin monomers. A number of hydrophobic residues on the apposing faces of actin and myosin contribute to the main binding site. This site is flanked on three sides by charged myosin surface loops that form predominantly ionic interactions with adjacent regions of actin. Hydrogen bonding is likely to play a significant role in actin–actin and actin–myosin interactions since many of the contacts involve loops. The model building approach used with actomyosin is applicable to other multicomponent assemblies of biological interest and is a powerful method for revealing molecular interactions and providing insights into the mode of action of the assemblies.**

Filamentous actin (f-actin) and myosin are, respectively, the track and motor components that comprise one of the major systems for molecular movement in the cell. To understand how these two molecules accomplish mechanochemical coupling, it is necessary to have a detailed description not only of their atomic structures but also of the way in which they interact at various stages during the work cycle. Three-dimensional crystals of the track or of the track–motor complex are not available, presumably because of the difficulty in crystallizing a linear polymer of variable length. In addition, attempts to cocrystallize monomeric actin and the myosin head have been unsuccessful. Structural information on actin–actin and actin–myosin interactions cannot therefore be obtained by x-ray crystallographic methods directly.

To obtain this information, a combination of approaches has been required. First, x-ray crystallography has provided the atomic structures of the individual components: vertebrate myosin subfragment 1 (S1) and the scallop regulatory (light-chain binding) domain have been crystallized and solved to high resolution (1, 2). The atomic structure of actin has been obtained from cocrystals of actin–DNase I, profilin–actin, and gelsolin segment 1–actin (3–5). Second, EM and image analysis of f-actin and actomyosin rigor complexes have revealed the locations, packing arrangement, and geometry of interaction of the filament components as well as information on the dynamic nature of some interactions (6–10). Third, x-ray fiber diffraction of oriented gels of f-actin was used to obtain high-resolution diffraction data on the filaments (11). Finally, the results obtained from all these approaches were combined to build, test, and refine atomic models of the filaments (11–17).

The actomyosin complex is composed of actin, the myosin heavy chain, and two myosin light chains—the essential light chain and the regulatory light chain. The interactions I will describe in this brief review are (*i*) the proposed intermolecular contacts in the actin filament, (*ii*) the contacts between the myosin S1 heavy chain and the light chains, and (*iii*) the proposed contacts at the actin–myosin interface in the rigor complex. In each case, I will briefly outline the results and rationale that led to the models before focusing on the molecular interactions and their possible consequences.

Actin–Actin Contacts

The atomic structure of the actin–DNase I complex was solved 5 years ago (3). Subsequently, very similar actin structures were obtained from crystals of actin complexed with profilin (4) and with gelsolin segment 1 (5). Viewed in the standard orientation (Fig. 1, lowest actin monomer), the square-shaped molecule can be divided into four subdomains: subdomain 1 at bottom right (residues 1–32, 70–144, and 338–375), subdomain 2 at top right (residues 33–69), subdomain 3 at bottom left (residues 145–180 and 270–337), and subdomain 4 at top left (181–269) (see ref. 3). The nucleotide binding site lies roughly in the center.

An atomic model of f-actin was built to fit data obtained by x-ray fiber diffraction of oriented f-actin gels (11). The model has been refined with a directed mutation algorithm and using normal modes as refinement parameters (15, 17). The placement and orientation of the monomer in the filament model is consistent with the f-actin structure seen at ≈30 Å by EM and three-dimensional image analysis and with the location of a gold cluster label (attached to Cys^{374}) determined by EM difference mapping (7–10). There are some uncertainties regarding the exact positioning of the region containing the DNase I binding loop (residues 35–55) and the C-terminal helix (residues 368–375) (9, 10, 16, 17, 19). In addition, the loop containing residues 264–274 was rebuilt as an antiparallel β-sheet (11, 15, 17).

Each monomer in the filament makes contact with four others: the preceding and following monomers along the same long pitch strand (referred to as the lp − 1 and lp + 1 monomers, respectively) and the preceding and following monomers along the short pitch helix (sp − 1 and sp + 1, respectively) (Fig. 1). sp − 1 and sp + 1 lie in the second long pitch strand. The intermolecular interactions along the long pitch strand predominantly involve surface loops, so hydrogen bonding may play a significant role in the interactions. The four contacts at each molecular interface effectively bind subdomain 3 of one monomer to subdomains 2 and 4 of the lp − 1 monomer (Fig. 1, blue regions). The 320–328 loop lies close to the 241–247 loop in the monomer below (lp − 1). Both loops have a number of hydrophobic residues and have a complementary charge. The second interaction involves two loop–helix motifs: residues 282–295 and lp − 1 loop 197–209. Again hydrophobic and

The publication costs of this article were defrayed in part by page charge payment. This article must therefore be hereby marked "*advertisement*" in accordance with 18 U.S.C. §1734 solely to indicate this fact.

Abbreviations: f-actin, filamentous actin; S1, subfragment 1.

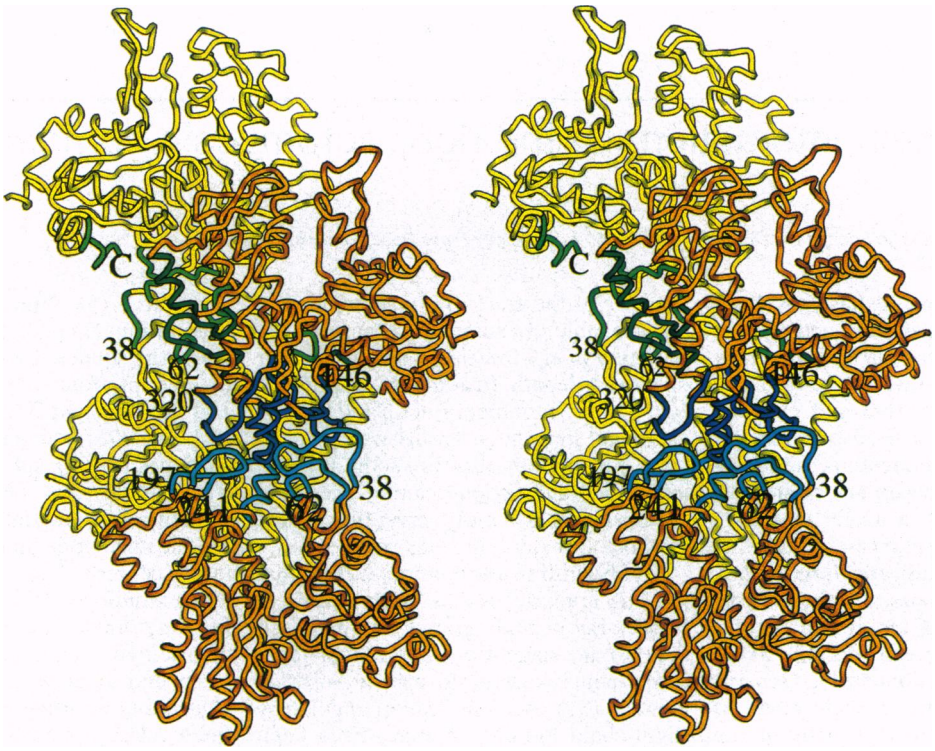

FIG. 1. Contacts between monomers in f-actin. Shown is a stereo pair of the polypeptide backbone of four filament monomers. One of the long pitch strands is yellow; the other strand is tan. Only the unique contacts are shown. Loops making long pitch intermolecular contacts are shown in dark blue (for lp0) and light blue (for lp − 1). Contacts between strands are shown in dark green (lp0) and light green (sp − 1 and sp + 1). Illustration was prepared using MOLSCRIPT (18).

charged residues are present. The third interaction pairs the loops protruding from β-sheet structures in subdomains 3 and 2: residues 162–176 and lp − 1 residues 38–52 (part of the DNase I binding loop). Hydrophobic residues constitute more than half the amino acids in each of these loops. The final interaction involves residues 146–148 (Gly-Arg-Thr) and 62–64 (Arg-Gly-Ile) in lp − 1.

Three regions of contact lie between the two long pitch strands (Fig. 1, green regions). The least extensive interaction involves loop 110–112 (Leu-Asn-Pro) and sp − 1 loop 195–197 (Glu-Arg-Gly). The most extensive interaction involves residues 261–275—a loop in the actin–DNase I structure that was rebuilt into an antiparallel β-sheet structure during refinement of the filament model. The resulting finger-like structure has a hydrophobic tip (Phe-Ile-Gly-Met) that lies between the monomers in the second long pitch strand (11, 15, 17). This interstrand contact involves portions of the polypeptide chain from three monomers: the finger from one monomer; loop 63–65 (Gly-Ile-Leu) and loop 38–40 (Pro-Arg-His) from the sp − 1 monomer; and loop 285–288 (Cys-Asp-Ile-Asp), loop 168–172 (Gly-Tyr-Ala-Leu-Pro), and loop 146–148 (Gly-Arg-Thr) from the sp + 1 monomer. These five regions of the polypeptide chain come together to form a hydrophobic pocket into which the hydrophobic fingertip is inserted. Although not shown in the model, the final region of contact for which there is some evidence (8, 9, 17, 19) is between helix 223–230 and the C-terminal helix (residues 368–375) of monomer lp + 1.

The f-actin model shows that each actin monomer uses 10 surface loops and two α-helices to make a large number of interactions with its four neighbors. During filament formation, a substantial movement of the C terminus is required to allow the two α-helices to interact. In addition, there is evidence that interactions involving the DNase I binding loop (residues 35–55) can change, depending on the divalent cations present or the state of the nucleotide bound (9, 10).

Interactions Involving the Light Chains

Myosin light chains share considerable structural homology with calmodulin; indeed, calmodulin serves as the light chain(s) in a number of unconventional myosins (1, 2, 20–22). Schematically, the light chains can be thought of as having a limited number of defining structural features: they have two hydrophobic pockets connected by a flexible linker or expansion joint, with divalent cation binding sites on the outsides of the pockets. Viewed in this way, it would seem logical that the pockets' structure and therefore their binding characteristics could be modulated by cation binding. Furthermore, the promiscuity of binding of calmodulin in particular can be explained by the flexibility of the linker between the pockets. Finally, the two-site attachment would allow for overall high-affinity binding of the molecule to the target.

The chicken skeletal muscle S1 structure and the structure of the regulatory domain of scallop myosin provide two detailed descriptions of the interactions between the light and heavy chains of myosin (1, 2) (Fig. 2). The target for light chain binding is an α-helix of the so-called IQ motif, a sequence of the general form IQXXXRGXXXRXXY/W (2, 23, 24). In the two structures solved, the target helix is very hydrophobic and most of these residues make contacts with the light chains. The critical element in the hydrophobic interaction appears to be the presence of long chain or aromatic hydrophobic residues separated by 12 amino acids (I and Y/W in the canonical sequence) (2, 21). These residues lie on opposite sides of the α-helix and are enclosed by the hydrophobic pockets of the C- and N-terminal domains of the light chains, respectively (Fig. 2 *Lower*). In the case of calmodulin, the expansion joint allows binding to a target helix in which the hydrophobic residues are separated by only eight amino acids (21).

There are roughly equal numbers of positively charged and negatively charged residues on the target α-helices. However, none of the negatively charged residues seems to participate in light-chain binding, whereas ≈50% of the positively charged

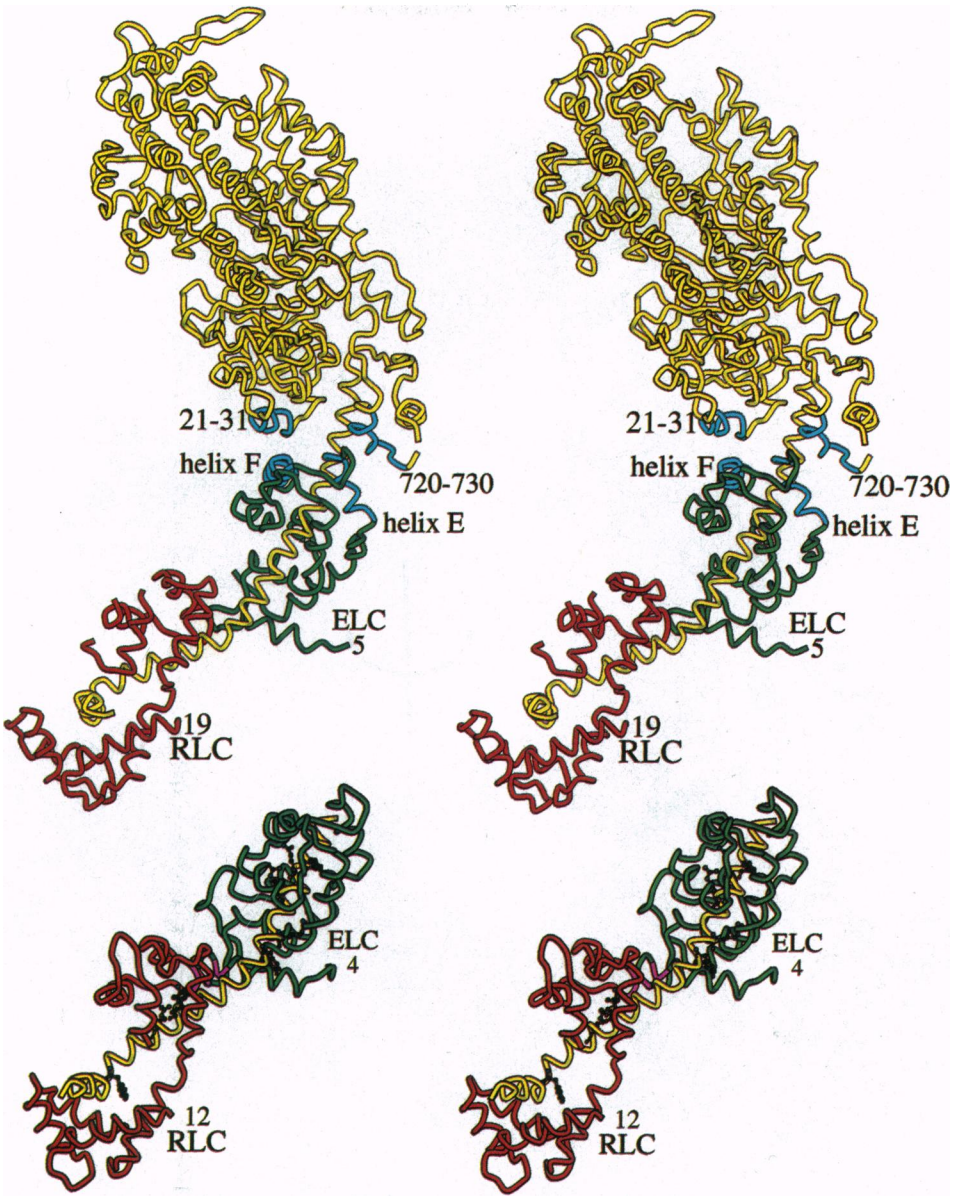

FIG. 2. Light-chain–light-chain and light-chain–heavy-chain interactions in the myosin head. Myosin heavy chains are yellow. Essential and regulatory light chains are green and red, respectively. (*Upper*) Stereo pair of the chicken skeletal myosin S1 structure (1). Interactions between the essential light chain and parts of the heavy chain other than the target α-helix are shown in light blue. (*Lower*) Stereo pair of the regulatory domain of scallop myosin (2), with ball and stick representations of some side chains in the IQ motifs. Contacts between the regulatory light chain (Gly^{117}) and the essential light chain (Phe^{20} and Arg^{24}) are shown in purple. Similar contacts probably occur in the vertebrate myosins. Illustration was prepared using MOLSCRIPT (18).

residues form salt bridges and/or hydrogen bonds with the light chains. Of the contacts between the light chains and the heavy chain, ≈10% are hydrogen bonds and ≈90% are van der Waals interactions (2). Similar figures have been reported for calmodulin bound to a synthetic target peptide (21). One of the more obvious differences in the binding of the two light chains is that the essential light-chain target α-helix is straight, whereas that of regulatory light chain has a >60° bend lying roughly between the two domains of this light chain (1, 2) (Fig. 2).

In the scallop myosin regulatory domain, two contacts between the light chains are required for Ca^{2+} triggering and regulation. Gly^{117} of the regulatory light chain participates in both contacts; its main-chain nitrogen is hydrogen bonded to the main-chain carbonyl oxygen of Phe^{20} of the essential light chain. Its main-chain carbonyl oxygen is similarly linked to the main-chain nitrogen of Arg^{24} in the essential light chain. These bonds bring Gly^{23} in the essential light chain and Gly^{117} in the regulatory light chain into close contact and stabilize the specific triggering Ca^{2+} binding loop in the essential light chain. The loop is further stabilized by additional interactions between the light and heavy chains (Fig. 2 *Lower*). Thus, binding of the triggering Ca^{2+} is critically dependent on contacts involving the heavy chain and both light chains (2).

Examination of the S1 structure suggests that there are contacts between the essential light chain and parts of the heavy chain other than the target helix (Fig. 2 *Upper*). Essential light-chain residues 90–96 form a helix just C-terminal to the expansion joint (corresponding to the E helix in calmodulin) and lie in close proximity to a short helix formed from heavy-chain residues 720–730. In addition, the next light-chain helix (helix F, residues 103–115) is close to a helix–loop motif near the N terminus of the heavy chain (residues 21–31). In light of recent structural data on myosin–nucleotide complexes (25), it would seem that these contacts may play a critical, if not pivotal, role in mechanochemical coupling.

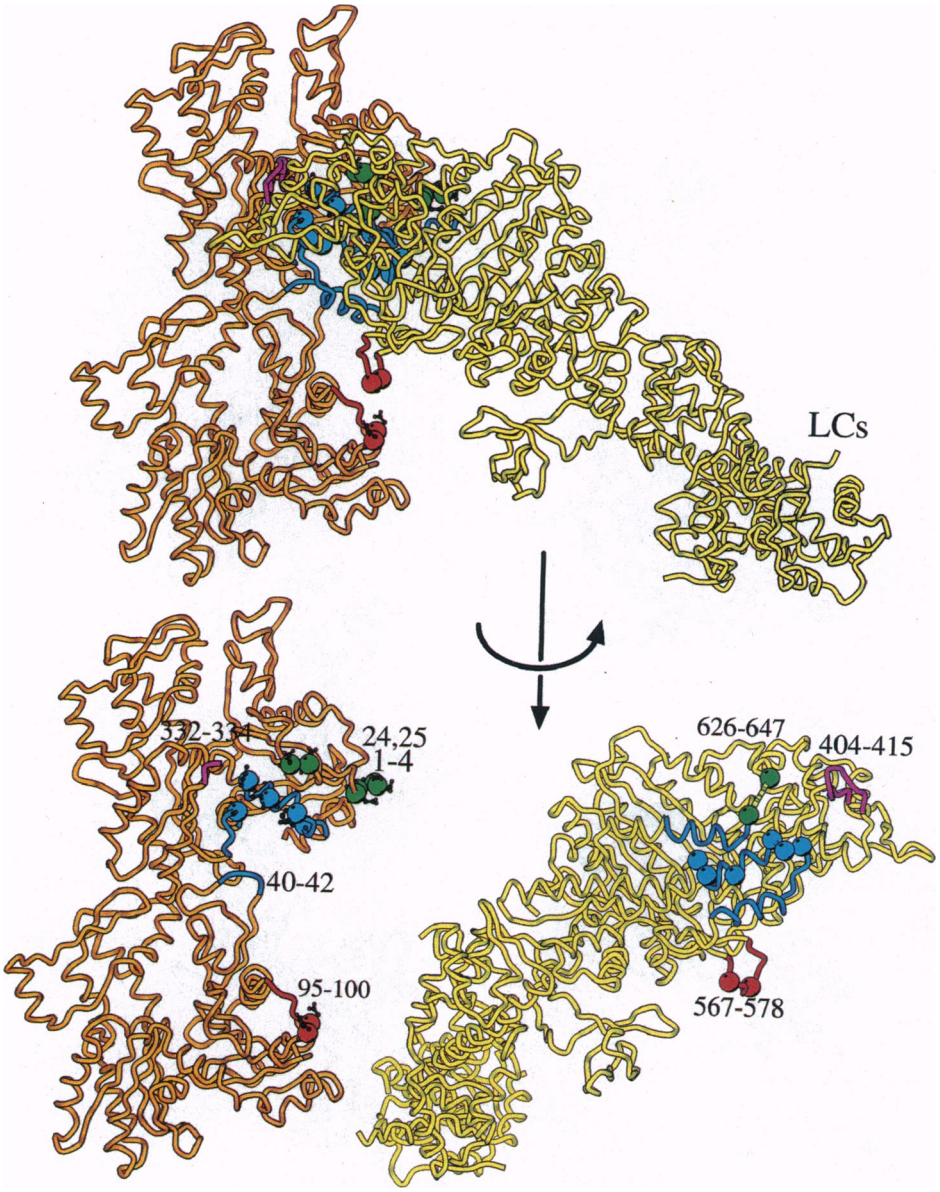

FIG. 3. Intermolecular interactions in the actomyosin rigor complex. (*Upper*) Two long pitch f-actin monomers interacting with the myosin head in the rigor conformation. Docking the x-ray structure with the f-actin model was carried out as described in ref. 13. (*Lower*) S1 has been rotated about a vertical axis to expose the surface that had been in contact with actin. Elements of the main binding site are shown in blue. Hydrophobic residues are represented by blue spheres. A lysine-rich loop comprising residues 626–647—the so-called 50k/20k loop—is not present in the x-ray structure. Residues 626 and 647 are represented by green spheres as are actin residues 1–4, 24, and 25, which are most likely involved in interactions with the loop. The so-called familial hypertrophic cardiomyopathy loop of myosin residues 404–415 and its putative contact site with actin residues 332–334 are shown in purple. Elements of the putative secondary binding site, myosin residues 567–578 and actin residues 95–100, are shown in red. Illustration was prepared using MOLSCRIPT (18).

Vertebrate striated muscle essential light-chain isoforms are of two types, the smaller of which is seen in the S1 structure. The larger isoform has an additional 41-amino acid residue extension at the N terminus. The presence of this isoform in muscle alters the maximum filament sliding velocity (e.g., see ref. 26). There is increasing evidence that a charged region of this N-terminal extension interacts with the C terminus of actin (refs. 7 and 25 and references therein). In the S1 structure, the N terminus of the essential light chain lies roughly in the center of the light chain, so the N-terminal extension of the larger isoform must span a distance of 70–80 Å along the underside of the S1 to reach the actin C terminus. Roughly half of the extension (in an extended conformation) is required to cover this distance, leaving a small domain of ≈20 amino acid residues to interact with the actin C terminus.

Actin–Myosin Rigor Interactions

The model of the actomyosin rigor complex was built from the f-actin filament model, the x-ray structure of S1, and three-dimensional maps of the rigor actomyosin complex obtained by cryoelectron microscopy and image analysis (1, 7, 11, 13, 14). Three types of essential information were obtained by electron microscopy (6, 7, 13, 14). First, three-dimensional maps calculated at a resolution of ≈30 Å revealed the overall shape of the complex and the geometry of actomyosin interaction. Second, difference analysis of three-dimensional maps of actomyosin containing and lacking the essential light chain revealed the location of the light chain in the complex. Third, the first 80 amino acids of the heavy chain were located by comparing two three-dimensional maps, one of which was of a myosin lacking this domain. Although all the three-dimensional maps had a resolution of ≈30 Å, the precision with which the light chain and

the N-terminal domain could be located in the three-dimensional maps was better than ≈5 Å. Thus, the shape of the complex, the location of specific protein components, and the location of a domain of one component provided sufficient constraints to allow the S1 atomic structure to be positioned and oriented uniquely with respect to the f-actin filament model (13, 14).

Even a relatively casual inspection of the resulting model shows that providing an exact description of the interactions at the actin–myosin interface is not an easy task. The strong constraints provided by the EM data necessitate placing the S1 in a position that results in a collision at the actin–myosin interface. It has been suggested that a conformational change in the S1—perhaps closure of the deep cleft in the molecule—would alleviate these steric problems and allow the two molecules to achieve a precise fit (13). It is not unreasonable to suspect that there may also be small changes in actin that contribute to the expected molecular complementarity. A second problem concerns a myosin surface loop—the so-called 50k/20k loop composed of residues 626–647. There is strong evidence that this loop participates in actomyosin interactions (27, 28). Unfortunately, these residues are not visualized in the x-ray structure and therefore they cannot be positioned with certainty on the actin surface. A similar situation occurs in part of another loop (Lys^{567}–His^{578}), which is a good candidate for an additional actomyosin interaction (7, 13). Although these attributes of the model effectively rule out an exact description of the actomyosin rigor interface, the most probable general features of the interaction can be described.

The rigor contact between actin and the myosin head can be divided into four distinct regions. A large primary binding site on the face of actin (Fig. 3, blue) is flanked on three sides by additional contacts involving myosin surface loops (13). The primary binding site is where the collision occurs in the model. The parts of the myosin molecule involved in the primary site are a helix–loop–helix motif (Pro^{529}–His^{558}) and part of an adjacent helix (Gln^{647}–Lys^{659}). These myosin secondary structure elements are in very close proximity to a helix–loop–helix near the C terminus of actin (Ile^{341}–Gln^{354}), a loop between Ala^{144} and Thr^{148} on the same monomer and part of the DNase I binding loop (His^{40}–Gly^{42}) on an adjacent monomer (lp − 1) in the filament. Although there are a number of potentially complementary ionic and polar groups, a notable feature of the binding site is the presence of a number of hydrophobic residues. Sandwiched between the actin and myosin in this region of the model are actin residues Ala^{144}, Ile^{341}, Ile^{345}, Leu^{349}, and Phe^{352}. They are close to residues Pro^{529}, Met^{530}, Ile^{535}, Met^{541}, Phe^{542}, and Pro^{543} of myosin (Fig. 3, blue spheres). While this primary binding region clearly involves hydrophobic interactions, ionic interactions and hydrogen bonding involving the peptide backbone in adjacent loops also seem likely.

The loops flanking this main binding site contribute additional contacts with actin. There is considerable evidence that the 50k/20k loop (Tyr^{626}–Gln^{647}) participates in actomyosin interactions (27, 28). In the S1 whose structure was solved, this loop contains five lysines and nine glycines and lies above the main binding site. In the model, this loop would be close to six negatively charged residues on the surface of actin (Asp^1, Glu^2, Asp^3, Glu^4, Asp^{24}, and Asp^{25}) (Fig. 3, green). It is therefore expected that the interaction would be predominantly ionic in nature.

Below the main binding site, the resolved portion of another charged loop (Lys^{567}–His^{578}) extends toward actin and is a good candidate for the so-called secondary binding site visualized in the EM maps (7, 13). Again, the interactions here are likely to be ionic since there are positively charged residues in the loop and they seem well positioned to interact with actin loop 95–100—possibly with Glu^{99} and Glu^{100} (Fig. 3, red).

The third loop (Pro^{404}–Lys^{415}) lies at the front or nose of the myosin molecule and is important for normal myosin activity (29, 30). A single amino acid change here in human β cardiac myosin (equivalent to an Arg^{405} to Gln change in the chicken sequence) is associated with familial hypertrophic cardiomyopathy (30). In the model, this myosin loop lies close to actin residues Pro^{332}–Glu^{334} (Fig. 3, purple).

In summary, the myosin rigor binding site on f-actin is extensive and spans the junction between two adjacent actin monomers in the long pitch helix. The binding site appears to be centered on hydrophobic interactions involving helices at the actin and myosin surfaces. Around this "greasy patch" in the main region of interaction there are complementary ionic and polar groups. Myosin surface loops flank this main region on three sides. The loops are well placed to allow ionic interactions with the surface of actin. It seems likely that hydrogen bonding involving the polypeptide backbone on adjacent loops contributes significantly to the binding site.

Conclusion

The interactions between the protein components of the actomyosin rigor complex are extensive. The x-ray structures of a vertebrate myosin S1 and of the scallop myosin regulatory domain provide a detailed picture of the way in which the light chains interact with the heavy chain and with each other. The general principles revealed are likely to hold true for light chain binding throughout the myosin family. A model building approach incorporating data from x-ray crystallographic, fiber diffraction, and EM studies has proved extremely successful in revealing the probable intermolecular contacts in f-actin and in the actomyosin rigor complex. In f-actin the bonding pattern appears to be complex and involves predominantly loop interactions along and between the actin long pitch strands. One interaction involves loops from three molecules. The interaction of actin and the myosin head in the rigor complex is very extensive, involving two actin monomers and four discrete parts of the apposing myosin face. There is evidence for direct binding of part of the large essential light-chain isoform to the C-terminal part of actin.

Construction of a high-resolution model of a macromolecular complex by combining moderate resolution EM data on the intact complex with the x-ray crystal structures of its individual components is a powerful approach for studying large multicomponent assemblies that are not amenable to crystallization or current x-ray crystallographic methods—e.g., virus–antibody and virus–receptor complexes, muscle filaments, motor–microtubule complexes, ribosomes, and nuclear pore complexes. Models built in this way reveal structural details of the interactions between components and provide insights into the mode of action of the assembly (13, 31).

I am grateful to my immediate colleagues for comments on the manuscript and for help in making the illustrations. R.A.M. is supported by grants from the National Institutes of Health (AR39155, GM44932, and GM52468) and is an Established Investigator of the American Heart Association.

1. Rayment, I., Rypniewski, W. R., Schmidt-Bäse, K., Smith, R., Tomchick, D. R., Benning, M. M., Winkelmann, D. A., Wesenberg, G. & Holden, H. M. (1993) *Science* **261,** 50–59.
2. Xie, X., Harrison, D. H., Schlichting, I., Sweet, R. M., Kalabokis, V. N., Szent-Györgyi, A. G. & Cohen, C. (1994) *Nature (London)* **368,** 306–312.
3. Kabsch, W., Mannherz, H. G., Suck, D., Pai, E. F. & Holmes, K. C. (1990) *Nature (London)* **347,** 37–44.
4. Schutt, C. E., Myslik, J. C., Rozycki, M. D., Goonesekere, N. C. W. & Lindberg, U. (1993) *Nature (London)* **365,** 810–816.
5. McLaughlin, P. J., Gooch, J. T., Mannherz, H.-G. & Weeds, A. G. (1993) *Nature (London)* **364,** 685–692.
6. Milligan, R. A. & Flicker, P. F. (1987) *J. Cell Biol.* **105,** 29–39.
7. Milligan, R. A., Whittaker, M. & Safer, D. (1990) *Nature (London)* **348,** 217–221.
8. Orlova, A. & Egelman, E. H. (1995) *J. Mol. Biol.* **245,** 582–597.

9. Orlova, A., Prochniewicz, E. & Egelman, E. H. (1995) *J. Mol. Biol.* **245,** 598–607.
10. Bremer, A., Henn, C., Goldie, K. N., Engel, A., Smith, P. R. & Aebi, U. (1994) *J. Mol. Biol.* **742,** 683–700.
11. Holmes, K. C., Popp, D., Gebhard, W. & Kabsch, W. (1990) *Nature (London)* **347,** 44–49.
12. Holmes, K. C., Tirion, M., Popp, D., Lorenz, M., Kabsch, W. & Milligan, R. A. (1993) in *Mechanism of Myofilament Sliding in Muscle Contraction*, eds. Sugi, H. & Pollack, G. H. (Plenum, New York), pp. 15–24.
13. Rayment, I., Holden, H. M., Whittaker, M., Yohn, C. B., Lorenz, M., Holmes, K. C. & Milligan, R. A. (1993) *Science* **261,** 58–65.
14. Schröder, R. R., Manstein, D. J., Jahn, W., Holden, H., Rayment, I., Holmes, K. C. & Spudich, J. A. (1993) *Nature (London)* **364,** 171–174.
15. Lorenz, M., Popp, D. & Holmes, K. C. (1993) *J. Mol. Biol.* **234,** 826–836.
16. Mendelson, R. A. & Morris, E. (1994) *J. Mol. Biol.* **240,** 138–154.
17. Tiron, M. M., ben-Avraham, D., Lorenz, M. & Holmes, K. C. (1995) *Biophys. J.* **68,** 5–12.
18. Kraulis, P. J. (1991) *J. Appl. Crystallogr.* **24,** 946–950.
19. Owen, C. & DeRosier, D. (1993) *J. Cell Biol.* **123,** 337–344.
20. Meador, W. E., Means, A. R. & Quiocho, F. A. (1992) *Science* **257,** 1251–1255.
21. Meador, W. E., Means, A. R. & Quiocho, F. A. (1993) *Science* **262,** 1718–1721.
22. Titus, M. A. (1993) *Curr. Opin. Cell Biol.* **5,** 77–81.
23. Mercer, J. A., Seperack, P. K., Strobel, M. C., Copeland, N. G. & Jenkins, N. A. (1991) *Nature (London)* **349,** 709–713.
24. Cheney, R. J. & Mooseker, M. S. (1992) *Curr. Opin. Cell Biol.* **4,** 27–35.
25. Fisher, A. J., Smith, C. A., Thoden, J., Smith, R., Sutoh, K., Holden, H. M. & Rayment, I. (1995) *Biophys. J.* **68,** 19s–28s.
26. Sweeney, H. L. (1995) *Biophys. J.* **68,** 112s–119s.
27. Mornet, D., Pantel, P., Audemard, E. & Kassab, R. (1979) *Biochem. Biophys. Res. Commun.* **89,** 925–932.
28. Uyeda, T. Q. P., Ruppel, K. M. & Spudich, J. A. (1994) *Nature (London)* **368,** 567–569.
29. Cuda, G., Fananapazir, L., Zhu, W. S., Sellers, J. R. & Epstein, N. D. (1993) *J. Clin. Invest.* **91,** 2861–2865.
30. Geisterfer-Lowrance, A. A. T., Kass, S., Tanigawa, G., Vosberg, H. P., McKenna, W., Seidman, C. E. & Seidman, J. G. (1990) *Cell* **26,** 999–1006.
31. Johnson, J. E. (1995) *Proc. Natl. Acad. Sci. USA* **93,** 27–33.